International Journal of Urology (2007) **14**, 96–103 doi: 10.1111/j.1442-2042.2007.01614.x

Imaging of renal and prostate carcinoma with refractive index radiology

Cheol Yong Yoon,[1] Duck Je Sung,[2] Ju Han Lee,[3] Ae Ri Kim,[3] Chil Whan Oh,[4] Jung Ho Je,[5] Byung Mook Weon,[5] Seung Kwon Seol,[5] Aram Pyun,[5] Yeukuang Hwu,[6] Giorgio Margaritondo,[7] Kwan Joong Joo[8] and Duck Ki Yoon[1]

Departments of [1]Urology, [2]Radiology, [3]Pathology and [4]Dermatology, College of Medicine, Korea University, and [8]Department of Urology, Kangbuk Samsung Hospital, Sungkyunkwan University School of Medicine, Seoul, and [5]Department of Materials Science and Engineering, Pohang University of Science and Technology, Pohang, Korea; [6]Institute of Physics, Academia Sinica, Nankang, Taipei, Taiwan; and [7]Faculté des Sciences de Base, Ecole Polytechnique Fédérale de Lausanne (EPFL), Lausanne, Switzerland

Aim: Having better edge enhancement and penetrating power, refractive index radiology is suitable for the imaging of weakly absorbing objects such as tissue specimens. In this study the potential of refractive index radiology was evaluated for the imaging of renal cell carcinoma (RCC) and prostate cancer (PCA).

Methods: Specimens were cut in 3 mm and 4 μm thickness for X-ray radiology and hematoxylin and eosin (HE) staining, respectively. Radiographic images of RCC and PCA were obtained using the synchrotron hard X-rays from the 7B2 beam-line of the Pohang Light Source (PLS). The imaging technique applied was phase-contrast radiology based on the refraction enhancement mechanism. The resulting radiographic images were analyzed in correlation with those of optical microscopy.

Results: Using unmonochromatized hard X-rays, it was possible to obtain images with clear edge enhancement and relatively large field of view (6 cm × 6 cm). Even with overlapping signals from thick samples (more than 700-fold thicker than microscopic images), radiographic images clearly showed histological information of organelles in normal kidney such as glomeruli, tubules, and collecting ducts. Histological information of RCC including tumor subtypes and minute changes such as cystic degeneration could be identified without difficulty. The radiographic images of the prostate were comparable with those of low magnification optical microscopy, providing good visualization of normal microstructures such as adenoma, smooth muscle, and normal glands, or differentiation of tiny tumors from surrounding normal tissues.

Conclusions: These results suggest the potential of refractive index radiology to provide a new way of imaging biological tissues with low absorption contrast such as RCC and PCA.

Key words: prostate cancer, refractive index radiology, renal cell carcinoma.

Introduction

Conventional X-ray imaging techniques generate contrast from differences in X-ray absorption determined by linear attenuation coefficients between tissues. Because the absorption differences between structures of soft tissues such as tumor and adjacent normal area are usually quite small, the resultant image contrast is relatively low.[1,2] Recently alternative contrast mechanisms that depend on the differences in refractive index rather than absorption coefficient have been developed.[3–7] When X-ray goes through an object, X-ray phase shift is generated due to the nature of its wave. The phase shift of a cross section can be 1000 times larger than the absorption of the cross section for hard X-rays.[7–9] Therefore, imaging techniques based on refractive index give far more advanced edge enhancement between soft tissues, making it possible to observe histological details even without additional contrast enhancing agents.[7,10] In this study we used strongly collimated synchrotron hard X-rays from the ICPCIR (International Consortium of Phase Contrast Imaging and Radiology) 7B2 X-ray microscopy beam-line at the Pohang Light Source (PLS) for the refraction-enhanced phase shifts generated.[7,11]

In addition to better edge enhancement, another advantage of hard X-ray (wavelength <1 Å) is its high penetration capability for soft tissues enabling the acquisition of better images from thick samples compared to soft X-rays.[12] Indeed, in a previous study we successfully visualized relatively thick biological samples (5 mm in thickness) with great lateral resolution using refractive index radiology.[13]

From a technical point of view the 7B2 beam-line has several unique aspects. One of these is the elimination of monochromator generating unmonochromatized X-rays, which lead to an increase in flux, resulting in several benefits such as large field of view (FOV), high flux, and real-time imaging.[4,7] These features suggest that the 7B2 beam-line is suitable for radiographic imaging of relatively thick and large biological samples with low absorption contrast.[14,15]

Despite these benefits, to date a limited number of studies has been carried out to image biological tissues such as tumors in internal organs using refractive index radiology. In this study we investigated the detailed appearance of refractive index radiographic images of two common urological malignancies, renal cell carcinoma (RCC) and prostate adenocarcinoma (PCA), comparing the images with those of optical microscopy to determine anatomical features as represented by refractive index radiology.

Methods

Instruments

The experiment was performed at the ICPCIR 7B2 beam-line of the PLS, as described previously.[15] The most important feature of the beam-line is that it uses unmonochromatized hard X-ray (10–60 keV), which is beneficial for the spatial and temporal resolution.[4,7] Figure 1

Correspondence: Duck Ki Yoon MD PhD, Department of Urology, Korea University, College of Medicine, 80 Guro-dong, Guro-gu, Seoul 152-703, Korea. Email: dkyoon@korea.ac.kr

Received 10 November 2005; accepted 20 June 2006.

© 2007 The Japanese Urological Association

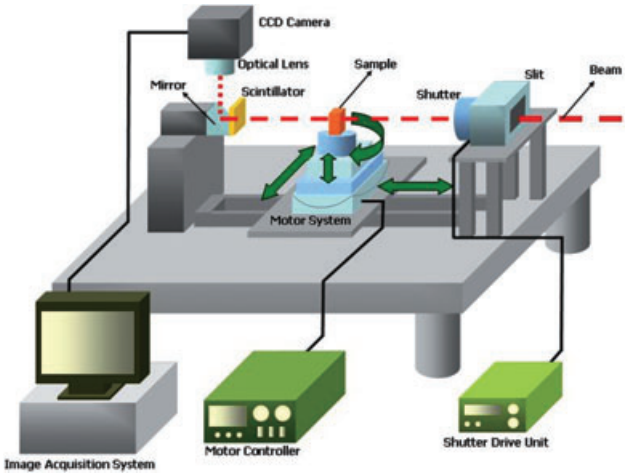

Fig. 1 Overall scheme of the PLS phase-contrast radiography system.

shows the refractive index radiology system. The experimental geometry and in particular the detector position were selected to emphasize the refraction-based mechanism. The radiology system consists of three main parts: attenuator, sample holder, and X-ray detector. The attenuator modifies not only the intensity but also the photon energy spectrum. The sample holder allows adjustment of three coordinates (with 0.1 µm accuracy) plus tilting and rotation (with 0.0009° and 0.002°). The longitudinal coordinate can be varied over a large range corresponding to object–detector distances from 15 mm to 1.5 m.

The transmitted X-rays are captured by a thin (200 µm) $CdWO_4$ double-polished single crystal scintillator and converted to a visible image. This image is then magnified by an optical lens (from ×3 to ×50) before being captured and stored by CCD camera (typically 1600×1200 pixels). The spatial resolution in our system reached 1 µm.

Specimen preparation and image acquisition

Paraffin blocks of 10 RCC specimens with various histological backgrounds (four conventional, three papillary, two chromophobe, and one collecting duct carcinoma) and one PCA specimen (organ-confined adenocarcinoma) were prepared as described in Table 1. Sections with thicknesses of 4 µm and 3 mm were cut from adjacent areas of each specimen for HE staining and refractive index imaging, respectively. For HE staining of PCA, the whole mount prostate section with 4 µm thickness was used after processing for paraffin fixation.

For refractive index imaging of the RCC specimens, the additional paraffin was melted and removed by placing the sections on 30°C heating plate for 10 min. The retrieved tissues were then wrapped with Kapton foils to prevent over-drying. For the PCA specimen, a formalin-fixed radical prostatectomy specimen with was first horizontally cut in 3 mm thickness with prostate base, and then placed between two layers of Kapton foil for refractive index imaging.

The RCC and the PCA specimens were then mounted on the sample holder. Optimum images were acquired by aligning the specimens using the sample holder with 3-D tilting and rotational functions and by adjusting the objective–detector distance. The objective–detector distance was optimally 15 cm in this experiment. In practice, the 7B2 beam-line has very large FOV up to 15×15 cm. In this study, the individual FOV was generally 8.5 mm but an overall large FOV of 6×6 cm was obtained, if necessary, by taking 49 small images (7×7 mm) and patching them together.

Results

Refractive index imaging of normal kidney

Figure 2a shows the refractive index radiographic image of normal renal cortex, displaying the typical features of a radiographic image of relatively thick biological samples. Small organelles in normal renal cortex such as glomeruli and surrounding proximal tubules are well identified with close similarity to that of low magnification optical microscopy (Fig. 2b). However, in contrast to the corresponding microscopic image, more glomeruli are visible in the radiographic image at similar magnifications. The tubules around the glomeruli also seem to be more densely packed in the radiographic image. These are assumed to be caused by the strong penetrating power of hard X-rays. Unlike conventional histological microscopy, which usually represents only single or a few cell layers, hard X-ray can penetrate relatively thick tissue specimens and generate signals from stacks of cells. Therefore the final images acquired by hard X-rays come from the projection of multiple cell layers resulting in visualization of multilayered cells and organelles in a single image.

Figure 2c is the radiographic image of the corticomedullary junction of normal kidney. In the lower left part of the image finely intermingled thread-like structures are visualized, corresponding to tubules in the juxtamedullary cortex. In addition, numerous parallel straight tubular structures are identified in the upper right part of the picture, indicating the collecting duct of medulla. Compared to the optical microscopic image (Fig. 2d) more densely packed tubules and ducts are also seen in the radiographic image.

Refractive index imaging of RCC

The radiographic image of a conventional RCC (Fig. 3a) demonstrates typical histological characteristics of this tumor. Even though the cell content looks coarser than that of the optical microscopy (Fig. 3b), probably due to projection of multiple cell layers, tumor cells still keep their clear cytoplasm and cell-to-cell boundaries. The tumor portion (right lower part of the image) is also well discriminated from the surrounding fibrous pseudocapsule (left upper part of the image).

Figure 3c shows the radiographic image of another conventional RCC. In the optical microscopy image (Fig. 3d), this tumor is seen to accompany massive cystic degeneration with mucinous material in it. Even with a relatively thick specimen prepared, these characteristic features are also well visualized in the radiographic image as homogenous lobulated areas with high signals (cystic lesions), surrounded by tumor cells with clear cytoplasm.

Figure 3e shows the radiographic image of a papillary RCC demonstrating the characteristic features of whirl-like structures in the central areas of tumor next to a peripheral portion with filicoid branching pattern. Nearly the same findings can be identified under optical microscopy examination (Fig. 3f).

Figure 3g is the radiographic image of a collecting duct RCC with sarcomatoid feature, showing a homogenous clump of densely packed cells without any intervening structures. This corresponds with the sarcomatoid portion of the tumor with a spindle-shaped fascicle forming area seen in the optical microscopic image (Fig. 3h). The

© 2007 The Japanese Urological Association

Table 1 Characteristics of patients with RCC and PCA

Patient no.	Sex	Age (years)	Tumor site	Size (cm)	Histological subtype	Nuclear grade†	Pathological stage
RCC							
1	M	44	Right	1.7	Conventional	II	pT1N0M0
2	M	42	Left	7.0	Conventional	II	pT2N0M0
3	M	41	Left	11.0	Conventional	III	pT2N0M0
4	F	68	Left	8.5	Conventional	IV	pT3aN0M0
5	M	63	Left	2.5	Papillary	III	pT1N0M0
6	M	27	Right	11.0	Papillary	II	pT2N0M0
7	F	42	Right	7.0	Papillary	III	pT3aN0M0
8	F	43	Right	8.0	Chromophobe	II	pT2M0M0
9	M	46	Left	9.0	Chromophobe	II	pT2N0M0
10	M	47	Right	11.5	Collecting ductal‡	III	pT2N0M0
PCA							
11	M	51	Right§	0.5	Adenocarcinoma	9 (4 + 5)	pT2aN0M0

†Fuhrman grade for RCC, Gleason sum for PCA; ‡collecting duct carcinoma with sarcomatoid feature; §tumor located at right peripheral zone.
F, female; M, male; PCA, prostate cancer; RCC, renal cell carcinoma.

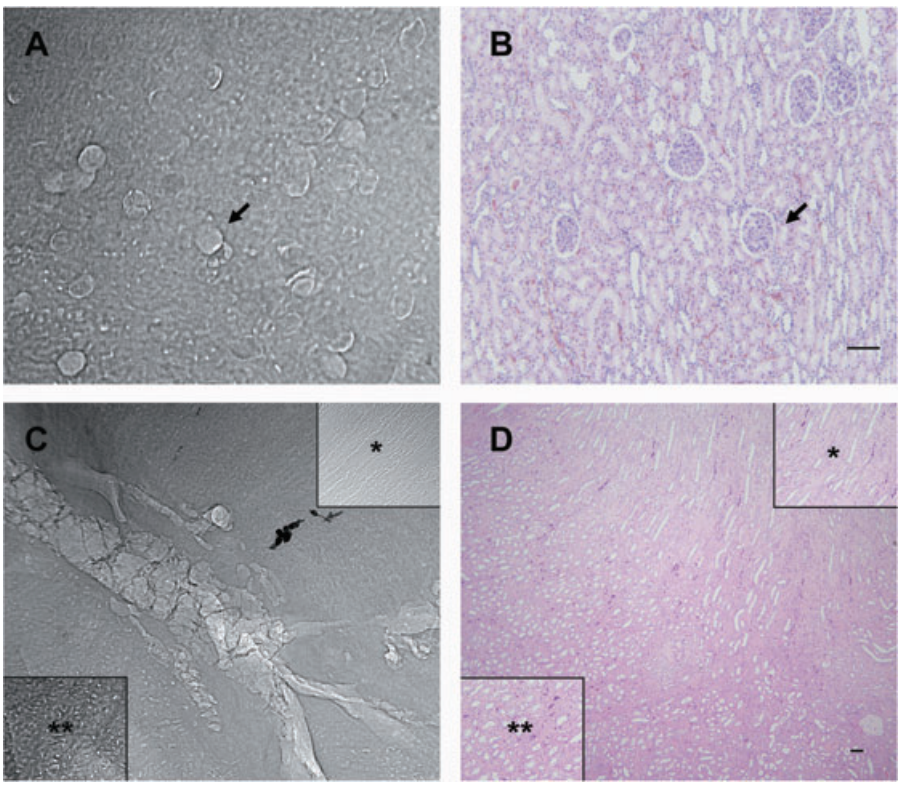

Fig. 2 Histological and phase-contrast images of normal kidney. Representative images of normal glomeruli (arrow) and adjacent proximal tubules by (a) phase-contrast imaging and (b) HE staining. Original magnification × 100. Images of collecting duct of medulla (asterisk) and tubules of juxtamedullary cortex (double asterisk) by (c) phase-contrast imaging and (d) HE staining. Original magnification × 40. Line bar = 200 μm.

typical histological characteristics of this tumor are tubule and duct forming areas admixed with a sarcomatoid component.

We also performed radiographic imaging of two chromophobe RCCs (data not shown). Although radiographic images of the normal areas of these specimens showed nearly the same findings as the other samples, the findings of the tumor areas were too different from those of optical microscopy to make a proper comparison between the two.

Refractive index imaging of whole mount prostate

Figure 4 is the radiographic image of a whole mount of the prostate with a resolution of 8691 × 6891 pixels in 14-bit gray color, which was generated by combining 49 small images (7 × 7) with the resolution of 1332 × 990 pixels. The gross appearance (Fig. 4) and its magnified image (Fig. 5) show the characteristic histological features of prostate very clearly.

© 2007 The Japanese Urological Association

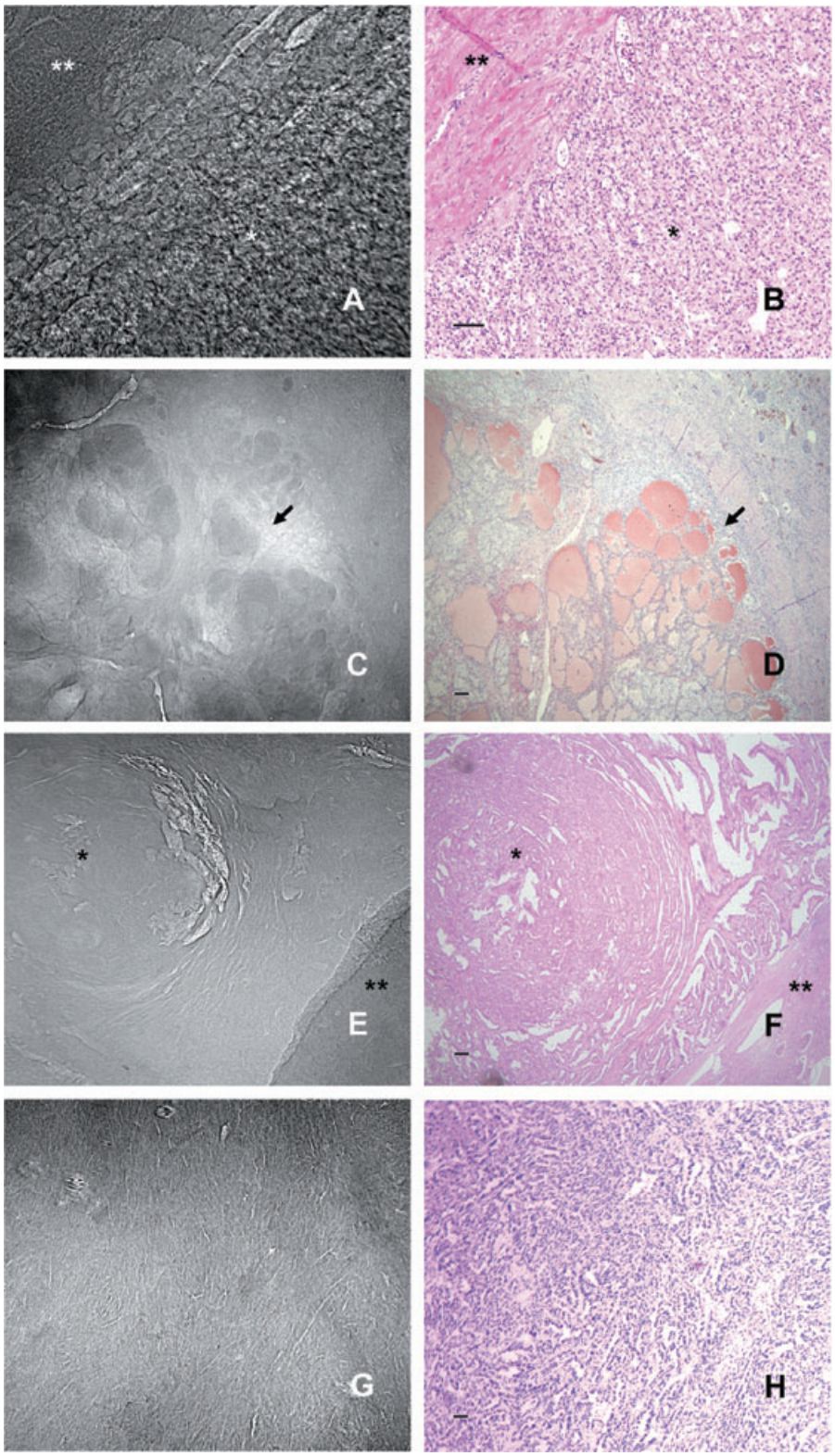

Fig. 3 Histopathological and phase-contrast images of renal cell carcinoma (RCC). Representative images of conventional RCC (asterisk, patient 3, Fuhrman grade III) and surrounding connective tissue (double asterisk) by (a) phase-contrast imaging and (b) HE staining. Original magnification × 100. Images of conventional RCC (patient 2, Fuhrman grade II) with cystic degeneration (arrow) by (c) phase-contrast imaging and (d) HE staining. Original magnification × 40. Representative images of papillary RCC (asterisk, patient 7, Fuhrman grade III) and adjacent normal renal parenchyme (double asterisk) by (e) phase-contrast imaging and (f) HE staining. Original magnification × 40. Images of collecting duct carcinoma with sarcomatoid feature (patient 10) by (g) phase-contrast imaging and (h) HE staining. Line bar = 200 μm.

In the central area around the prostatic urethra (Fig. 5a,a′) several well-developed benign adenomas are identified (Fig. 5b). In comparison to the histological image (Fig. 5b′), not only the presence of benign adenomas but also the microstructure inside the adenoma are demonstrated very clearly using radiographic imaging (Fig. 5b). In the peripheral area (Fig. 5c) the projected image of overlapping cystic structures must be normal glands of the peripheral zone when compared with the histological image of the corresponding area (Fig. 5c′). Compared to microscopic image, there seem to be more glands in the radiographic image. This might be the result of the projection of

© 2007 The Japanese Urological Association

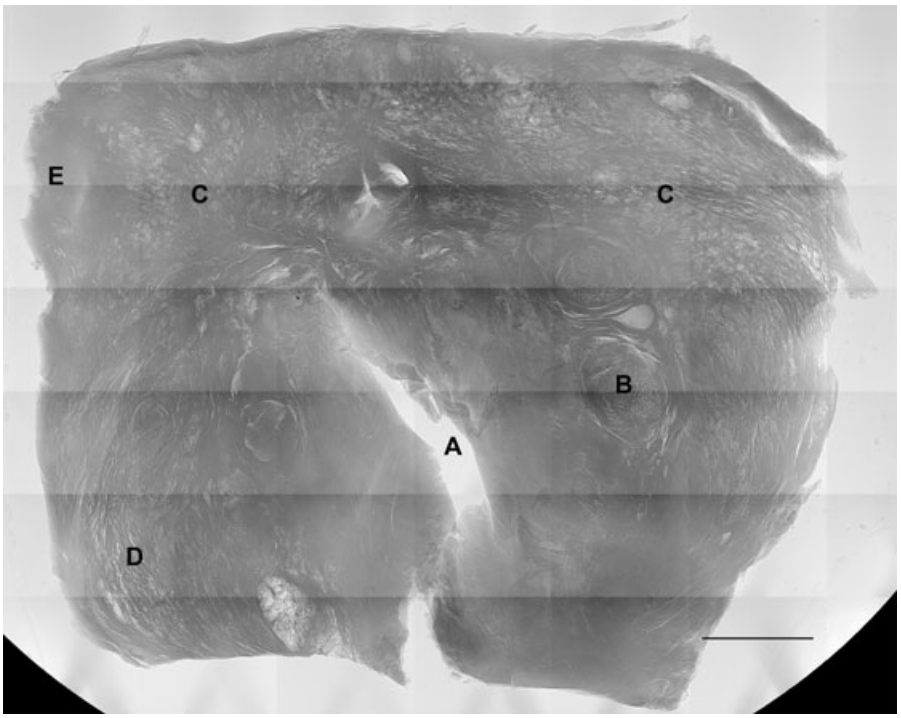

Fig. 4 Phase-contrast images of whole mount prostate section (3 mm in thickness, patient 11) from radical prostatectomy specimen of a patient with prostate adenocarcinoma (PCA): (a) urethra; (b) adenoma of transitional zone; (c) normal gland of peripheral zone; (d) anterior fibromuscular stroma (AFS) of prostate; (e) tumor at right peripheral zone. Line bar = 5 mm. Original resolution 8691 × 6891 pixels, original size 75.5 × 58.3 cm.

multiple layers at the same time by hard X-rays, as for RCC. However, in spite of the overlapping signals, basic cystic features of glands are identifiable without difficulty.

In the anterior portion of the specimen, striated structures with orientation (Fig. 5d) are demonstrated, very similar to the optical microscopic images of anterior fibromuscular stroma of the prostate in the corresponding area (Fig. 5d′). In this specimen, the tumor (Gleason sum 9) is located at the right peripheral zone (the left upper corner of Fig. 4). The tumor is organ-confined without invasion to the prostate capsule and is relatively tiny (only 5 mm in size). Even with this small size, the tumor area shows definitely different features from that of the surrounding normal glandular portion (Fig. 5e). When compared to the contralateral normal peripheral area (the right upper corner of Fig. 4), the difference becomes more obvious.

Discussion

Refractive index radiology is a kind of non-interferometric refraction enhanced imaging technique that depends on changes of refractive index in the samples for the visualization of phase information, and is considered as a good candidate for the imaging of weakly absorbing specimens.[16] Either synchrotron radiation or a microfocus X-ray source can be used for refractive index radiology.[17,18] However, a microfocus X-ray source should either use a screen with a small pinhole aperture or increase the source–sample distance to minimize the penumbra-like effect caused by large source size and angular spread.[3,4,13] Either of these technical modifications greatly reduce the X-ray flux reaching to sample.[19] However, synchrotron radiation is emitted from a source that is small in size and also strongly collimated, not requiring any additional manipulation to get spatial and temporal coherence. As a result, synchrotron hard X-rays generated have much better optimal conditions for the imaging of relatively thick biological specimens with low contrast.

There have been a few attempts to apply X-ray radiography to biological specimens such as cultured cancer cell lines and internal organs of laboratory animals.[8,20–26] One example is the successful visualization of the branching patterns of the normal bronchial tree and individual acinus of mice lung by diffraction enhanced imaging (DEI).[8,20] However, in the clinical field, its application has been limited to several specific disease entities in the form of synchrotron mammography and two-wavelength angiography (dichromography). Until recently there have been few studies using refractive index radiology for the exploration of tumors of internal organs such as RCC and PCA.[20–25] Takeda *et al*.[26] successfully demonstrated that the phase-contrast X-ray computed tomography technique can be used to visualize various histological features of human hepatocellular carcinoma and colon cancer. They were able to achieve a high spatial resolution of 12 μm even using a 5-mm thick specimen. Using the phase-contrast X-ray imaging technique based on the unmonochromatized hard X-rays from the third generation synchrotron radiations, Hwu *et al*.[13] recently suggested the possibility of this technique for the imaging of biological specimens as thick as 5 mm with clear histological information. They showed stomata in the epidermis of an aloe leaf as they opened up without staining in real-time.

In this study we considerably improved the resolution of the refractive index radiology by using hard X-ray from the 7B2 X-ray microscopy beam-line with high flux and sufficient penetrating depth and successfully explored the histological details of human RCC and PCA specimens. The beam-line has a very large FOV of up to 15 × 15 cm, which is superior to the recent record of the latest FOV (6 × 3 cm) by interferometry technique.[26–28] Refractive index radiology in most of the RCC samples detailed features of tumors including histological subtypes, and subtle morphological changes such as small cystic degeneration were identified with fair clarity. Refractive index radiology successfully visualized benign histological features of the prostate such as normal gland, smooth muscle components, and benign adenoma with optical microscopic detail. A tiny tumor (less than 5 mm in

© 2007 The Japanese Urological Association

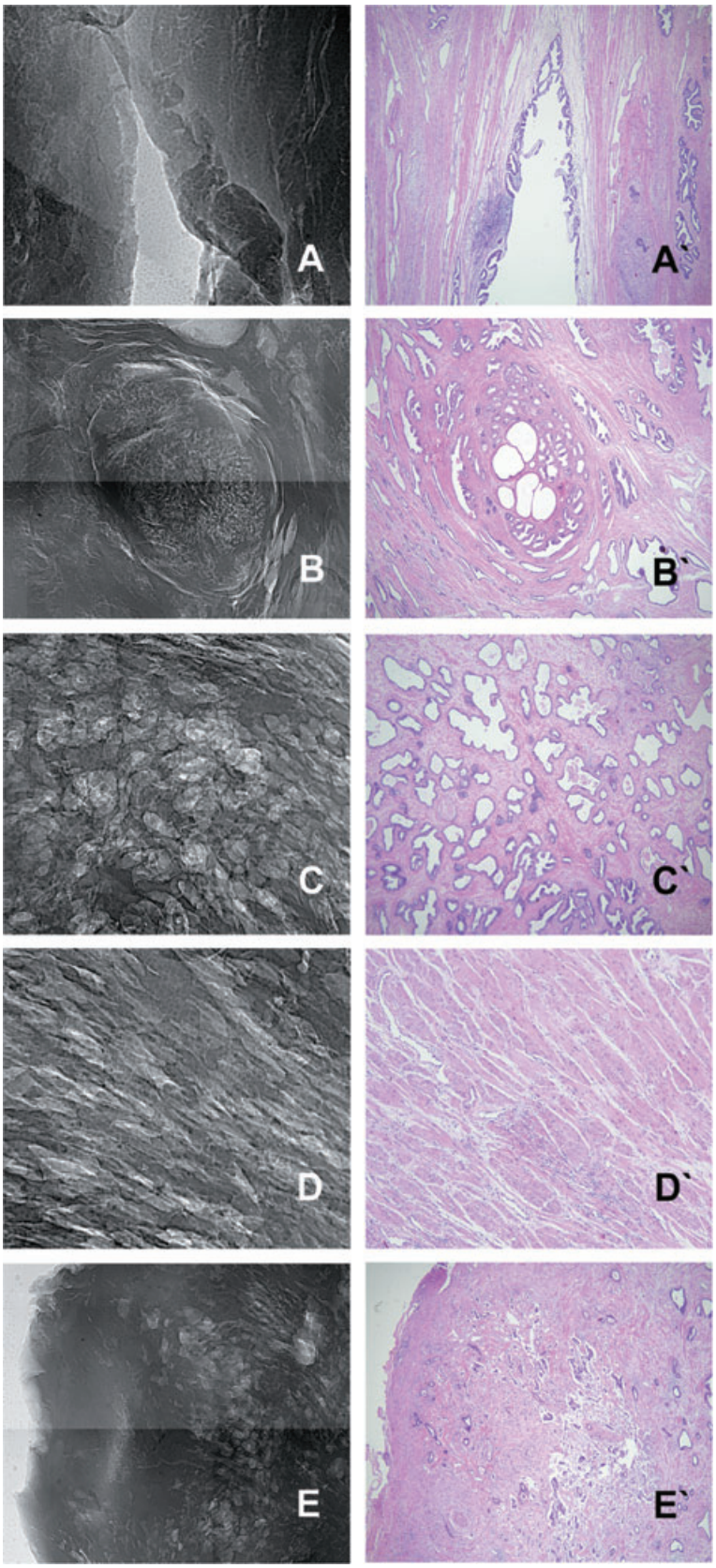

Fig. 5 Magnified phase-contrast and corresponding HE staining images of prostate: (a) and (a′) urethra; (b) and (b′) adenoma of transitional zone; (c) and (c′) normal gland of peripheral zone; (d) and (d′) anterior fibromuscular stroma (AFS) of prostate; (e) and (e′) tumor at right peripheral zone.

© 2007 The Japanese Urological Association

diameter) was also discriminated without difficulty. These results suggest that refractive index radiology has considerable resolution, enough to obtain proper histological information from thick tissue samples.

As mentioned already, due to the strong penetration capability of hard X-rays, refractive index radiology can be used for the imaging of relatively thick biological samples. Herein we used specimens of 3 mm thickness. Compared to the 4 μm thickness of conventional histological preparations, phase-contrast X-ray imaging of tissues with 3 mm thickness is analogous to obtaining images from hundreds of overlapping histological slides. Our results demonstrated that the histological characteristics including normal and pathological findings of kidney and prostate could be identified even with such thick samples. This indicated that the phase-contrast X-ray imaging enables us to obtain collective information of thick biological samples in a realistic environment without complicated preparation. It is also possible to reveal cellular details even in thick (3 mm) samples, by adopting 3-D microtomographic study,[13] which is under way for RCC and PCA.

Despite these advantages, at this point refractive index radiology is definitely not without limitations. For example using refractive index radiology we could visualize most major subtypes of RCC (conventional, papillary, collecting duct) with their characteristic histological features. However, in the case of chromophobe RCC, the findings acquired by refractive index radiology were somewhat different from those of optical microscopy and it was nearly impossible to infer histological information from the radiographic images. Because the number of specimens we tested in this work was limited we do not know if such an unexpected result is prone to happen in all cases of chromophobe RCC. Nevertheless, these results suggest that there are variations in findings of radiographic images according to histological type. Even though the thickness of 3 mm is much greater than that of conventional histological preparation, it is still a long way away from the penetrating depth required for clinical extracorporeal imaging. In addition, the blurring of images by overlapping signals from increasing sample thickness will need to be overcome before the clinical application of refractive index radiology.

We expect that most of these problems can be managed by advances in radiographic technique. For example in a previous study we successfully obtained images of biological specimens showing cellular level details at selective depths from the sample surface by combining refractive index radiology and tomographic reconstruction techniques.[13] We also successfully visualized tubules and ducts of the mouse kidney in its entirety (unpubl. data) and the coronary artery of living animals without contrast enhancing agents using the 3-D tomography technique of refractive index radiology.[29] These findings mean that not only blurring of images by overlapping signals from multiple cell layers but also limitation of imaging depth could be overcome by tomographic reconstruction.

To the best of our knowledge this is the first report about the application of synchrotron hard X-ray refractive index radiology to common urological malignances, RCC and PCA. We successfully demonstrated that cancerous lesions could be clearly differentiated from normal tissues and characteristic histological features of these tumors were well identified using refractive index radiology. We suggest that through technical advances such as tomographic reconstruction we could make this technique clinically applicable in the near future.

Acknowledgments

This research was supported by grants from the MOST (KOSEF) through the National Core Research Center for Bio-Dynamic Systems and through the SKORE-A program, by the Korea Ministry of Commerce, Industry, and Energy, and the Korea Industrial Technology Foundation (KOTEF).

The support of the ITEP (Korea Institute of Industrial Technology Evaluation & Planning) is gratefully acknowledged.

This research was supported by KUOS specialized programs of basic research in Genitourinary Cancer.

References

1 Momose A, Takeda T, Itai Y. Blood vessels: depiction at phase-contrast X-ray imaging without contrast agents in the mouse and rat: feasibility study. *Radiology* 2000; **217**: 593–6.
2 Wernick MN, Wirjadi O, Chapman D *et al.* Multiple-image radiography. *Phys. Med. Biol.* 2003; **48**: 3875–95.
3 Meuli R, Hwu Y, Je JH, Margaritondo G. Synchrotron radiation in radiology: radiology techniques based on synchrotron sources. *Eur. Radiol.* 2004; **14**: 1550–60.
4 Hwu Y, Shieh HH, Liu MJ *et al.* Coherence-enhanced synchrotron radiology: refraction versus diffraction mechanisms. *J. Appl. Phys.* 1999; **86**: 4613–18.
5 Chapman D, Thomlinson W, Johnston RE *et al.* Diffraction enhanced X-ray imaging. *Phys. Med. Biol.* 1997; **42**: 2015–25.
6 Tsai WL, Hsu PC, Hwu Y *et al.* Electrochemistry: building on bubbles in metal electrodeposition. *Nature* 2002; **417**: 139.
7 Margaritondo G, Hwu Y, Je JH. Synchrotron light in medical and materials science radiology. *Riv. Nuovo Cimento* 2004; **27**: 1–40.
8 Lewis RA, Hall CJ, Hufton AP *et al.* X-ray refraction effects: application to the imaging of biological tissues. *Br. J. Radiol.* 2003; **76**: 301–8.
9 Takeda T, Momose A, Wu J *et al.* Vessel imaging by interferometric phase-contrast X-ray technique. *Circulation* 2002; **105**: 1708–12.
10 Suzuki Y, Yagi N, Uesugi K. X-ray refraction-enhanced imaging and a method for phase retrieval for a simple object. *J. Synchrotron Radiat.* 2002; **9**: 160–5.
11 Wu X, Liu H. A new theory of phase-contrast x-ray imaging based on Wigner distributions. *Med. Phys.* 2004; **31**: 2378–84.
12 Miao J, Ishikawa T, Johnson B, Anderson EH, Lai B, Hodgson KO. High resolution 3D x-ray diffraction microscopy. *Phys. Rev. Lett.* 2002; **89**: 0883031–4.
13 Hwu Y, Tsai WL, Chang HM *et al.* Imaging cells and tissues with refractive index radiology. *Biophys. J.* 2004; **87**: 4180–7.
14 Hwu Y, Tsai WL, Groso A, Margaritondo G, Je JH. Coherence-enhanced synchrotron radiology: simple theory and practical applications. *J. Phys. D Appl. Phys.* 2002; **35**: R105–20.
15 Baik S, Kim HS, Jeong MH *et al.* International consortium on phase contrast imaging and radiology beamline at the Pohang Light Source. *Rev. Sci. Instrum.* 2004; **75**: 4355–8.
16 Chapman D, Pisano E, Thomlinson W *et al.* Medical applications of diffraction enhanced imaging. *Breast Dis.* 1998; **10**: 197–207.
17 Bronnikov AV. Theory of quantitative phase-contrast computed tomography. *J. Opt. Soc. Am. A Opt. Image Sci. Vis.* 2002; **19**: 472–80.
18 Gureyev TE, Stevenson AW, Paganin D *et al.* Quantitative methods in phase-contrast x-ray imaging. *J. Digit. Imaging* 2000; **13**: 121–6.
19 Donnelly EF, Price RR, Pickens DR. Quantification of the effect of system and object parameters on edge enhancement in phase-contrast radiography. *Med. Phys.* 2003; **30**: 2888–96.
20 Kitchen MJ, Paganin D, Lewis RA, Yagi N, Uesugi K, Mudie ST. On the origin of speckle in x-ray phase contrast images of lung tissue. *Phys. Med. Biol.* 2004; **49**: 4335–48.
21 Pisano ED, Johnston RE, Chapman D *et al.* Human breast cancer specimens: diffraction-enhanced imaging with histologic correlation – improved conspicuity of lesion detail compared with digital radiography. *Radiology* 2000; **214**: 895–901.
22 Arfelli F, Bonvicini V, Bravin A *et al.* Mammography with synchrotron radiation: phase-detection techniques. *Radiology* 2000; **215**: 286–93.

© 2007 The Japanese Urological Association

23 Kotre CJ, Birch IP. Phase contrast enhancement of x-ray mammography: a design study. *Phys. Med. Biol.* 1999; **44**: 2853–66.
24 Hasnah MO, Zhong Z, Oltulu O *et al.* Diffraction enhanced imaging contrast mechanisms in breast cancer specimens. *Med. Phys.* 2002; **29**: 2216–21.
25 Arfelli F, Assante M, Bonvicini V *et al.* Low-dose phase contrast x-ray medical imaging. *Phys. Med. Biol.* 1998; **43**: 2845–52.
26 Takeda T, Momose A, Hirano K, Haraoka S, Watanabe T, Itai Y. Human carcinoma: early experience with phase-contrast X-ray CT with synchrotron radiation – comparative specimen study with optical microscopy. *Radiology* 2000; **214**: 298–301.
27 Yoneyama A, Takeda T, Tsuchiya Y *et al.* A phase-contrast X-ray imaging system – with a 60×30 mm field of view – based on a skew-symmetric two-crystal X-ray interferometer. *Nucl. Instrum. Methods* 2004; **A523**: 217–22.
28 Momose A, Takeda T, Itai Y, Yoneyama A, Hirano K. Phase-contrast tomographic imaging using an X-ray interferometer. *J. Synchrotron Radiat.* 1998; **5**: 309–14.
29 Hwu Y, Tsai WL, Je JH *et al.* Synchrotron microangiography with no contrast agent. *Phys. Med. Biol.* 2004; **21**: 501–8.

© 2007 The Japanese Urological Association